ACS APPLIED BIO MATERIALS

Article

Stealth Polydopamine-Based Nanoparticles with Red Blood Cell Membrane for the Chemo-Photothermal Therapy of Cancer

Haijun Wang, Gareth R. Williams, Xiaotian Xie, Meng Wu, Junzi Wu, and Limin Zhu

ACS Appl. Bio Mater., **Just Accepted Manuscript** • DOI: 10.1021/acsabm.0c00094 • Publication Date (Web): 26 Feb 2020

Just Accepted

is published by the American Chemical Society. 1155 Sixteenth Street N.W., Washington, DC 20036

Stealth Polydopamine-Based Nanoparticles with Red Blood Cell Membrane for the Chemo-Photothermal Therapy of Cancer

Haijun Wang[1], Gareth R. Williams[2], Xiaotian Xie[1], Meng Wu[1], Junzi Wu[3*], Li-Min Zhu[1*]

[1] College of Chemistry, Chemical Engineering and Biotechnology, Donghua University, Shanghai, 201620, China

[2] UCL School of Pharmacy, University College London, 29-39 Brunswick Square, London, WC1N 1AX, UK

[3] College of Basic Medicine, Yunnan University of Chinese Medicine, Kunming, 650500, China

* Corresponding authors: E-mail: lzhu@dhu.edu.cn (Li-Min Zhu); beached@126.com (Junzi Wu)

Abstract: Herein, we developed curcumin (Cur)-loaded porous poly(lactic-co-glycolic acid) (pPLGA) nanoparticles (NPs) by the nanoprecipitation method. Dopamine (DA) was then self-polymerized to form a polydopamine (PDA) layer on the surface of the NPs, yielding Cur@pPLGA/PDA NPs able to act as both chemotherapeutic and photothermal agents. These NPs were further camouflaged with the red blood cell membrane (RBCM) to construct RBCM-Cur@pPLGA/PDA NPs. The RBCM-pPLGA/PDA NPs were around 200 nm in size, demonstrated photothermal performance in the NIR region with a potent photothermal conversion efficiency (35.2%). The blank carrier has favorable cytocompatibility, but when drug loaded can efficiently induce the death of cancer cells (particularly when combined with an NIR laser treatment). Cellular uptake results revealed greater *in vitro* uptake of RBCM-Cur@pPLGA/PDA NPs than bare Cur@pPLGA/PDA NPs in the case of cancer cells, but reduced macrophage phagocytosis. *In vivo* studies in mice showed the RBCM-Cur@pPLGA/PDA NPs exhibited prolonged blood circulation times and superior photothermal effect (>43 ℃) for tumor specific chemo-photothermal therapy. The RBCM-Cur@pPLGA/PDA NP platform presents great potential for targeted synergistic cancer treatments.

Keywords: Red blood cell membrane, Biomimetic, Polydopamine, Curcumin, Chemo-photothermal therapy

Introduction

Photothermal therapy (PTT) has attracted much attention currently because it offers the potential for non-invasive cancer treatment without off-target toxicity. PTT relies on the photothermal conversion of across visible to near-infrared (NIR) light into heat, with the latter used to drive local tumor ablation. If the process is well controlled, this can be done with minimal heating damage to adjacent healthy tissues. To progress PTT, extensive research has been undertaken into effective NIR light absorbing agents such as graphene oxide [1, 2], gold nanostructures [3, 4], copper chalcogenides [5], , and MoS_2 [6]. However, there are a number of problems with using such materials. Most, particularly those based on inorganic nanoparticles (NPs) are not biodegradable, which means there is a potential risk of accumulation *in vivo*. Further, the heating produced by the incident NIR beam is focused on a central point and decreases moving away from this. Hence, cancerous cells some distance from the focus of the beam may be damaged but not killed by the hyperthermia induced. To address these challenges, combining multiple therapies into a single formulation can be considered, for instance in chemo-photothermal therapy. This augments PTT with chemotherapy to improve the efficiency of cancer treatment [7].

Polydopamine (PDA) is a versatile surface coating agent which has recently drawn substantial research interest [8-10]. PDA is a naturally occurring melanin-like substance and exhibits excellent biocompatibility, rendering it promising for potential clinical applications [11]. PDA also effectively absorbs NIR over a broad spectral range [9, 12]. However, PDA-based nanoparticles (NPs) often face problems with poor stability *in vivo*. Much recent approaches have focused on using hydrophilic, neutral charged surface modifiers such as poly(ethylene glycol) (PEG) to address these issues [13, 14]. Unfortunately, PEG surface functionalization can also impede NP uptake by cancerous cells [15].

There is thus a need to improve NP stability while also maintaining or enhancing cellular uptake.

One possible approach to this challenge is to use cell membrane biomimetic nanocarriers [16]. These possess excellent biocompatibility, immunomodulatory effect, prolonged systemic circulation and endogenous tumor-targeting ability [17-21]. Systems derived from red blood cells (RBCs) have been particularly explored in medicines development [22]. They enjoy prolonged systemic circulation times, and since they are endogenous cells with inherent biocompatibility and low immunogenicity [23-25]. Therefore, using the RBC membrane (RBCM) to coat drug delivery systems (DDSs) is a powerful approach to realize enhanced therapeutics [23, 24]. The immunomodulatory protein CD47 presented on the RBCM sends "*don't eat me*" signals to macrophages [26]. Consequently, RBCM-cloaked materials can serve as considerable drug carriers *in vivo*, avoiding phagocytosis and achieving enhanced passive targeting of tumors [27-29].

In this work, we report RBCM-biomimetic PDA-based nanoparticles, as shown in Scheme 1. First, porous NPs based on the biodegradable polymer poly(lactide-co-glycolide) (PLGA) and loaded with the anti-cancer drug curcumin were developed. A PDA layer was then deposited on the surface of the Cur@pPLGA NPs. Subsequently, the particles were cloaked with the RBCM, giving RBCM-Cur@pPLGA/PDA NPs. The formulations were characterized in detail and their potential in cancer therapy explored both *in vitro* and *in vivo*.

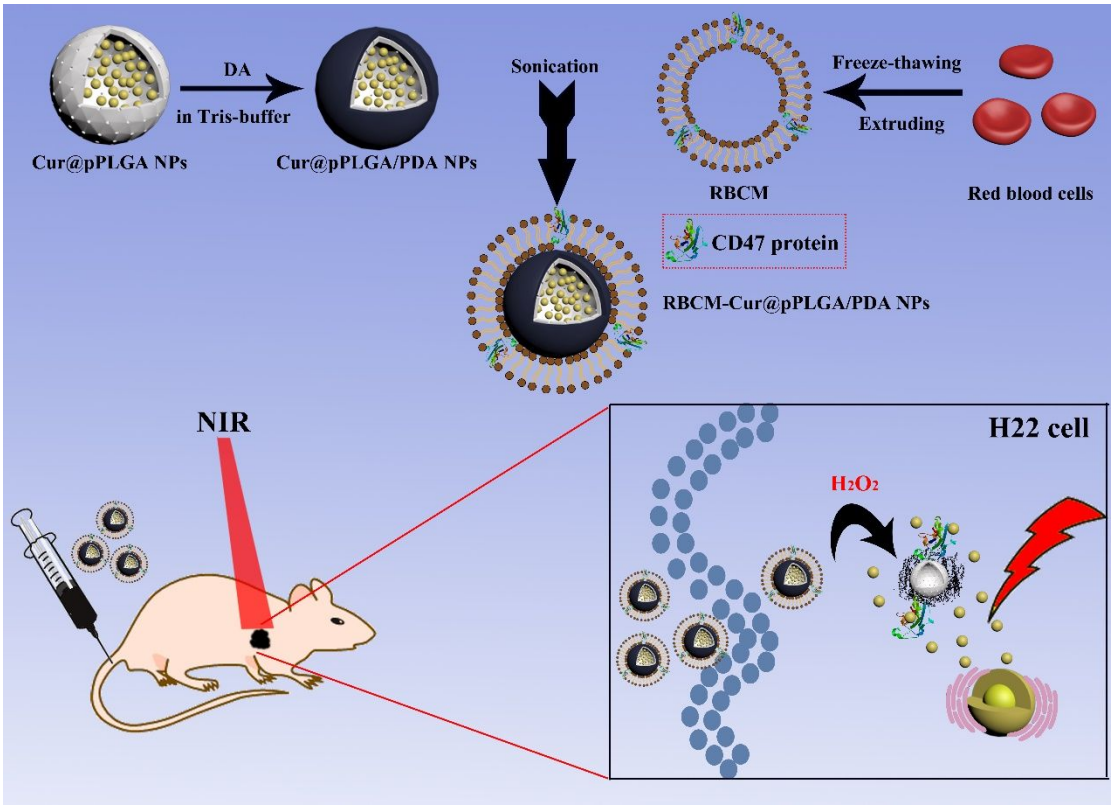

Scheme 1. The preparation of RBCM-Cur@pPLGA/PDA NPs and *in vivo* chemo-photothermal therapy.

EXPERIMENTAL SECTION

Materials and Reagents. PLGA (lactide: glycolide 50:50, Mw = ~21,000) was procured from Jinan Daigang Biological Engineering Co., Ltd. (Jinan, China). Curcumin, dopamine hydrochloride, tris(hydroxymethyl)aminomethane, dimethylsulfoxide (DMSO), H_2O_2 (30% v/v) and vitamin E polyethylene glycol succinate (TPGS) were purchased from Aladdin (Shanghai, China). Hoechst 33342, 3-(4,5-dimethylthiazol-2-yl)-2,5-diphenyl-tetrazolium bromide (MTT) were purchased from Sigma-Aldrich (St. Louis, MO, USA). Protease inhibitor and membrane protein extraction kit were procured from Phygene Life Sciences (Fuzhou, China). Dulbecco's Modified Eagle medium (DMEM), fetal bovine serum (FBS), phosphate buffered saline (PBS, pH = 7.4), penicillin,

streptomycin and trypsin-EDTA were obtained from Gibco (Carlsbad, CA, USA). A TUNEL staining kit was obtained from Wuhan Servicebio Technology Co., Ltd (Wuhan, China). H22 (murine hepatocellular carcinoma), RAW264.7 (murine macrophage) and L929 (mouse fibroblast) cells were provided by the Type Culture Collection of the Chinese Academy of Sciences (Shanghai, China). All other reagents and chemicals were used as obtained without further purification.

Preparation of Cur@pPLGA/PDA NPs. Drug-loaded porous PLGA (pPLGA) NPs were prepared using the nanoprecipitation method, as described previously [30]. Briefly, 50 mg curcumin, 20 mg TPGS and 100 mg PLGA were dissolved in 10 mL acetone. The obtaining mixture was added into 50 mL of deionized water under stirring. The Cur@pPLGA NPs were collected after centrifugation and washed repeatedly with deionized water to remove TPGS and create a porous structure. The supernatant was collected and diluted with methanol. Finally, the curcumin loading was quantified using a UV-vis spectrophotometer based on the curcumin calibration curve (in water). The curcumin encapsulation efficiency (EE %) and loading content (LC %) were calculated as follows:

$$\text{EE\%} = \frac{\text{mass of curcumin in NPs}}{\text{total mass of curcumin in feed}} \times 100\%$$

$$\text{LC\%} = \frac{\text{mass of curcumin in NPs}}{\text{total mass of NPs}} \times 100\%$$

The precipitate was re-dispersed in Tris-buffer (100 mL), and dopamine hydrochloride (DA•HCl) (100 mg) added under stirring (400 rpm) for 3 h. Any unreacted DA was removed by centrifugation, resulting in Cur@pPLGA/PDA NPs. Blank pPLGA and pPLGA/PDA NPs were prepared using the same procedures as above but omitting curcumin. In all cases, the pPLGA suspensions were freeze dried to prepare dry powers. The surface area and pore size of these were measured by automated Area and Pore size analyzer (Autosorb-iQ, Quantachrome Instruments, Boynton Beach, FL, USA).

Preparation of RBCM-Cur@pPLGA/PDA NPs. Fresh whole mouse blood was firstly extracted from female SD mice (specific pathogen-free grade, 180-200 g) were obtained from Shanghai SLAC Laboratory Animal Co., Ltd (Shanghai, China). The whole blood was transferred into an anticoagulant-coated tube and centrifuged (3000 rpm) for 5 min at 4 °C. The precipitate was collected after discarding the plasma and leukocytes coat, then washed with PBS three times. The resultant RBCs underwent a freeze-thaw process to induce membrane rupture. The released hemoglobin was removed by repeated centrifugation (4,000 rpm) at 4 °C until the supernatant was colorless. The resultant RBCMs were stored in PBS (pH = 7.4) containing protease inhibitor (2 mM) at −80 °C for further use.

RBCM-Cur@pPLGA/PDA NPs were prepared following a literature protocol [31]. 4 mL of a 2 mg/mL aqueous suspension of Cur@pPLGA/PDA NPs was mixed with RBCM derived from 1 mL of whole blood under magnetic stirring for 30 min, followed by a sonication process (40 kHz, 100 W) for 5 min obtaining RBCM-Cur@pPLGA/PDA NPs. Drug-free RBCM-pPLGA/PDA NPs were prepared using the same protocol but with pPLGA/PDA NPs as the starting material.

Characterization. Zeta potential and dynamic light scattering (DLS) data on the pPLGA, pPLGA/PDA, Cur@pPLGA/PDA and RBCM-Cur@pPLGA/PDA NPs were measured using a Zetasizer Nano ZS system (Malvern Instruments, Malvern, UK). Transmission electron microscopy (TEM) images were obtained using a JEOL 2010F instrument (Hitachi, Tokyo, Japan). UV-vis absorption spectra were collected on a UV-1800 spectrophotometer (UNICO, Shanghai, China). X-ray photoelectron spectroscopy (XPS) was undertaken on an Escalab 250Xi instrument (ThermoFisher, Waltham, MA, USA). Fourier transform infrared (FT-IR) spectra were acquired with a Nexus 870 spectrometer (Nicolet Instruments Inc., Madison, WI, USA).

RBCM protein analysis. The cell membrane proteins present in the RBCM-Cur@pPLGA/PDA NPs were assessed by the SDS-PAGE electrophoresis assay. The NPs were first centrifuged at 16,000 rpm in 10% w/v aqueous sucrose for 30 min, and proteins extracted using a Membrane Protein Extraction kit before separation by SDS-PAGE. Purified RBCM was used as a control, and all samples were normalized for equal protein concentrations using a Pierce BCA protein assay kit. The key immunomodulatory protein CD47 in RBCM was further examined by western blotting. Mouse anti-human CD47 was used as a primary antibody, with goat anti-rat HRP-conjugated secondary antibodies.

Photothermal effects. To measure the photothermal conversion efficacy, 1 mL of RBCM-Cur@pPLGA/PDA NPs suspensions at concentrations ranging from 0.1 to 2.0 mg/mL were charged into an Eppendorf tube and exposed to NIR laser irradiation (808 nm, 1 W/cm^2) for 5 min. The influence of the laser power density was ascertained by irradiating 1 mL suspension of RBCM-Cur@pPLGA/PDA NPs (1.0 mg/mL) under different power densities from 0.5 to 2.0 W/cm^2. To further determine the thermal stability, the materials was irradiated at 1.5 W/cm^2 for 5 min over five on–off cycles. In addition, the temperature of a RBCM-Cur@pPLGA/PDA suspension (1 mg/mL) was monitored under continuous NIR laser irradiation at 1 W/cm^2 for 10 min using an infrared thermal imaging system (GX-A300, Shanghai Guixin Corporation, Shanghai, China). Blank PBS was employed as a control. The photothermal conversion efficiency of RBCM-Cur@pPLGA/PDA was calculated using the following equation:

$$\eta = \frac{hS(T_{max} - T_{am}) - Q_0}{I(1 - 10^{-A})}$$

where h is the heat transfer coefficient, S is the surface area, T_{max} is the maximum equilibrium temperature, T_{am} is the ambient surrounding temperature and I is the laser power. A is the absorbance

of the sample solution at 808 nm, and Q_0 represents the heat absorption of the quartz cell.

Drug release. PDA-based NPs can be degraded by H_2O_2 [32]. Interestingly, compared to normal cells, the tumor cells overexpress H_2O_2 at a generation rate of 5 nmol/10^5 cells per hour [33]. The effect of H_2O_2 and temperature (given that this will rise in PTT) on the release behavior of the formulations was thus investigated. 2.0 mL of a 2 mg/mL suspension of RBCM-Cur@PLGA/PDA NPs was loaded into the dialysis bag (Mw = 8000-14000 kDa) and then suspended in PBS (18 mL) with or without H_2O_2 at a concentration of 10 mM. The samples were incubated at 37 °C or 45°C with shaking (120 rpm). At pre-determined time, Aliquots (n=3) were withdrawn from the external medium and an equal volume of fresh pre-heated buffer was replaced into the release system. The amount of curcumin released was determined by UV-vis spectroscopy at λ_{max} of 425 nm.

Cellular uptake. The uptake of Cur@pPLGA/PDA and RBCM-Cur@pPLGA/PDA NPs was observed using a confocal laser-scanning microscope (CLSM; LSM 700, Carl Zeiss, Oberkochen, Germany) equipped with an argon blue laser light (488 nm). RAW 264.7 or H22 cells were incubated at 37 °C for 24 h. The cells were then treated with 200 μg/mL Cur@pPLGA/PDA or RBCM-Cur@pPLGA/PDA suspensions in PBS. After another 2 h incubation, the cells were washed twice with PBS, and 1 mL of glutaraldehyde (2.5%) was added. After kept for 15 min at 4 °C, the cell nuclei were counterstained with 0.5 mL Hoechst 33342 (10 μg/mL) for 5 min and observed by CLSM.

Flow cytometry analysis was also performed. The H22 cells were incubated in six-well plates for 24 h. After removal of the medium, 1.8 mL of FBS-free DMEM and 200 μL of PBS or suspensions of Cur@pPLGA/PDA and RBCM-Cur@pPLGA/PDA NPs (2 mg/mL) were added, and the cells cultured for another 4 h. The cells were detached with 0.25% w/v trypsin-EDTA and

collected by centrifugation (3000 rpm, 3 min). The pellet dispersed in 500 μL of PBS after discarding supernatant. Finally, the cellular uptake was determined by flow cytometry.

Cytocompatibility and cytotoxicity. MTT assay was used to evaluate the cell viability. L929 cells and H22 cells were seeded into each well of a 96-well plate at a density of 1×10^4 cells / well, and incubated for 24 h. To evaluate the cytocompatibility of pPLGA/PDA and RBCM-pPLGA/PDA NPs, the initial incubation the medium was replaced with 200 μL of fresh medium containing different concentration of RBCM-pPLGA/PDA NPs, and the cells were further cultured for 24 h.

For cytotoxicity experiments, after the first 24 h culture period the initial medium was discarded and H22 cells treated with fresh medium containing free Cur, Cur@pPLGA/PDA, RBCM-Cur@pPLGA/PDA or RBCM-Cur@pPLGA/PDA in combination with exposure to an 808 nm laser. Laser irradiation (1 W/cm^2, 5 min) was applied 2 h after adding the formulations to the cells. Experiments were performed at a range of Cur concentrations.

For both cytocompatibility and cytotoxicity work, after the cells had been exposed to the formulations for 24 h, the cell viability was assessed using a MTT assay according to previous protocols [20].

***In vivo* murine tumor model**. All animal experiments were conducted with full authorization approved by the Committee for Experimental Animal Welfare and Ethics of Yunnan University of Traditional Chinese Medicine. 40 ICR female mice (SPF grade, 18–20 g) were acquired from Jiangsu KeyGEN BioTECH Co. Ltd (Nanjing, China). Tumors were developed by subcutaneous injection of H22 cells (1×10^6) dispersed in 100 μL of PBS into the right front limb armpit of each mouse.

NIR imaging *in vivo*. For these experiments, after H22 cell inoculation, the tumors were allowed

to grow to ~200 mm^3 in volume (calculated as length × $width^2/2$). Mice were then randomly divided into two groups (n = 3) receiving intravenous injections of (1) 200 μL PBS; (2) 200 μL RBCM-Cur@pPLGA/PDA NPs (2 mg/mL) in PBS. Mice were anesthetized 24 h post-injection [9], and then given 10 min of laser irradiation (808 nm, 1 W/cm^2) focused on the tumor. At given time points, NIR images were monitored and imaged with a FLIR Automated & Scientific Camera.

***In vivo* antitumor efficacy and safety evaluation**. When tumor volume reached ca. 60 mm^3 after H22 cell implantation, the mice were then randomly divided into five treatment groups (5 mice per group): (1) PBS; (2) free curcumin; (3) Cur@pPLGA/PDA NPs; (4) RBCM-Cur@pPLGA/PDA NPs; (5) RBCM-Cur@pPLGA/PDA NPs + laser. All groups bar group (1) received a curcumin dose of 2 mg/kg by intravenous injection every two days. The tumors in group (5) were additionally irradiated with an 808 nm NIR laser (1W/cm^2) for 5 min 24 h after injection. The tumor volumes and body weight were recorded every two days.

After 16 days, blood (0.5 mL) was withdrawn from three mice in each group *via* heart puncture. The blood samples were centrifuged (3500 rpm, 15 min) at 4 °C to obtain serum. The alanine aminotransferase (ALT), aspartate aminotransferase (AST), creatinine (CREA), and urea nitrogen (BUN) was then analyzed by an automatic biochemistry analyzer (Hitachi, Tokyo, Japan).

All the mice were then sacrificed, and the tumors and major organs were immediately excised and performed for H&E staining. Tumor tissues were further studied with TUNEL staining.

***In vivo* pharmacokinetics**. Swiss mice (8 weeks old, n=3) were obtained from Jiangsu KeyGEN BioTECH Co. Ltd and intravenously injected with a suspension of Cur@pPLGA/PDA or RBCM-Cur@pPLGA/PDA NPs in PBS (dose of Cur: 2 mg/kg). At predetermined time points, 20 μL blood samples were extracted from the ocular vein and dispersed in lysis buffer (0.5 mL; 1% w/v SDS, 1%

w/v Triton X-100, 40 mM tris acetate) for fluorescence measurements at 530 nm. The data were then normalized for ease of presentation. Pharmacokinetic parameters were calculated based on fitting a two-compartment model.

RESULTS AND DISCUSSION

Preparation and characterization of NPs. TEM images of the Cur@pPLGA NPs show the spherical morphology (Figure 1a). Their small size means that the pores cannot be resolved in the image, but nitrogen absorption measurements confirmed them to have porosity with most pores < 6 nm in size (see Figure S1, Supporting Information). In a weakly alkaline and aerobic conditions, dopamine molecules can be self-polymerized to form a PDA layer at the exterior of the Cur@pPLGA NPs. This can be seen in Fig. 1b, where a thin layer on the surface of the Cur@pPLGA NPs is clearly observed. The PDA coating is also clear from the FT-IR spectra given in Figure S2. In addition to PLGA vibrations, the spectrum of the PDA coated particles shows additional absorption bands at *ca.* 750 cm^{-1}, 1500 cm^{-1}, and 1600 cm^{-1}. These are ascribed to the benzene ring of PDA. Additional evidence for PDA coating is seen in XPS spectra (see Figure S3). The pPLGA/PDA NPs showed a distinct N1s peak at ~399.6 eV, while pPLGA displayed no peaks in this region.

After RBCM cloaking by sonicating a mixture of Cur@pPLGA/PDA NPs and RBCM fragments, an additional membrane structure could be observed around the periphery of the Cur@pPLGA/PDA NPs (Figure 1c). The zeta potentials of the pPLGA NPs and pPLGA/PDA NPs are approximately −15 mV and −25 mV respectively (Figure 1d), while after RBCM coating the latter is raised slightly to *ca.* −20 mV. This value is essentially the same as that of the RBCM itself (−19 mV). SDS-PAGE electrophoresis revealed that the protein composition of the RBCM was

largely preserved in the RBCM-Cur@pPLGA/PDA NPs (Fig. S4a). Western blotting results (Figure S4b) exhibit CD47 bands with both RBCM and RBCM-Cur@pPLGA/PDA NPs. This immunomodulatory protein hides cells from immune detection by sending "*don't eat me*" signals to macrophages, and its presence indicates the RBCM should provide stealth properties to the NPs.

The hydrodynamic size of Cur@pPLGA NPs was found to be 164 ± 8 nm, while the Cur@pPLGA/PDA analogue lies at 190 ± 5 nm and the RBCM-Cur@pPLGA/PDA NPs have sizes of 220 ± 4 nm, as determined by DLS (Figure 1e). As increasing layers of surface coating are applied, the NPs thus become larger, as would be expected. The coated RBCM-Cur@pPLGA/PDA NPs could be dispersed in DMEM buffer without aggregation over time, exhibiting considerable stability. In contrast, the Cur@pPLGA/PDA NPs aggregated severely after 2 h (Figure S5). The RBCM coating clearly imparts the formulation with much improved storage stability.

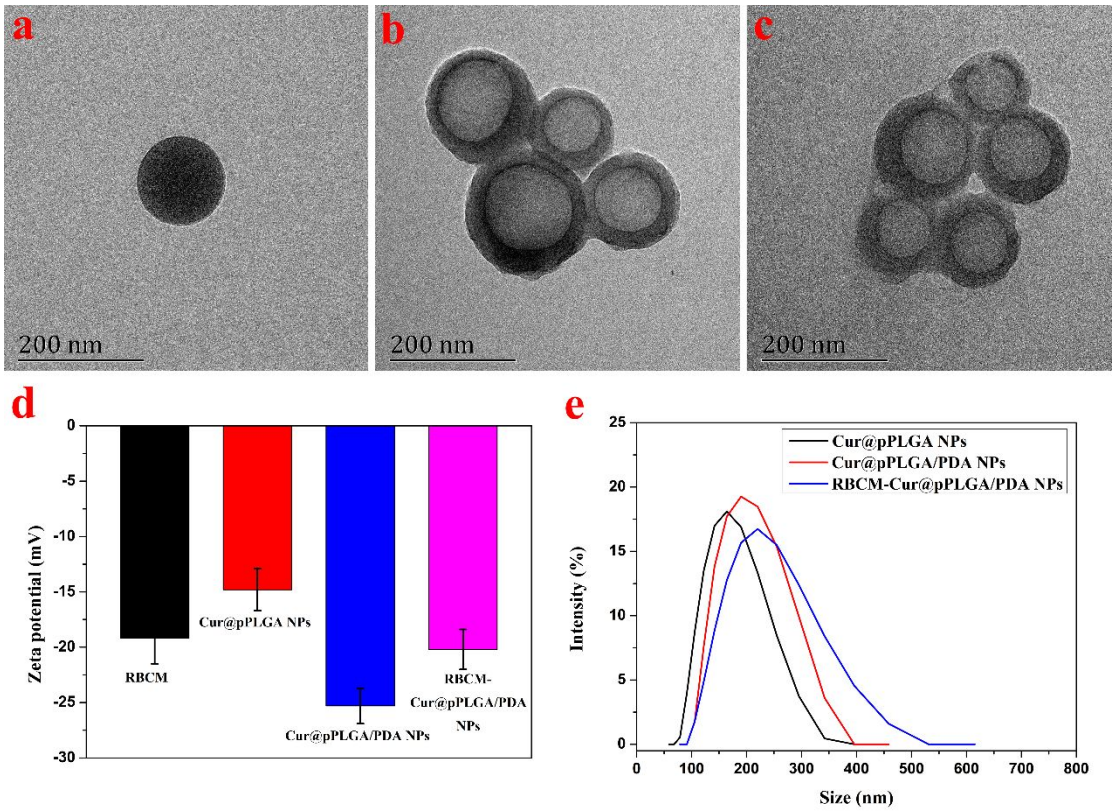

Figure 1. Characterization data for the NPs. TEM images of (a) Cur@pPLGA, (b)

Cur@pPLGA/PDA and (c) RBCM-Cur@pPLGA/PDA NPs; (d) Zeta potential values of the RBCM, Cur@pPLGA, Cur@pPLGA/PDA and RBCM-Cur@pPLGA/PDA NPs at pH=7.4; (e) DLS sizes of the NPs in water.

Photothermal effects. The photothermal conversion efficiency of PDA-based NPs was systematically investigated. As shown in Figure 2a, the RBCM-Cur@pPLGA/PDA aqueous solution displayed a concentration-dependent photothermal heating effect. A temperature increases to 53.8 °C was observed at a concentration of 2 mg/mL under irradiation (1 W/cm^2) for 5 min, while the temperature of PBS only increased by 1.5 °C under the same conditions. Using a suspension at 1.0 mg/mL an increase of laser power density ranged from 0.5 to 2.0 W/cm^2 (Figure 2b) also led to notable and power-dependent rises in temperature. The photothermal conversion efficiency of the RBCM coated NPs at 808 nm was calculated to be 35.2%. This is notably higher than reported in most literature studies, for instance with Au nanorods (η = 21%) [34] or semiconducting polymer conjugates (η = 20%) [35]. The dispersion shows excellent photothermal stability over five on/off cycles of laser irradiation (Figure 2c). Photothermal heating photographs recorded using an IR camera (Figure 2d) confirm these findings visually. After irradiation for 10 min, the temperature of the suspension increased up to 52.4 °C (see Figure 2e), showing the formulation to have potential for PTT treatment of cancer.

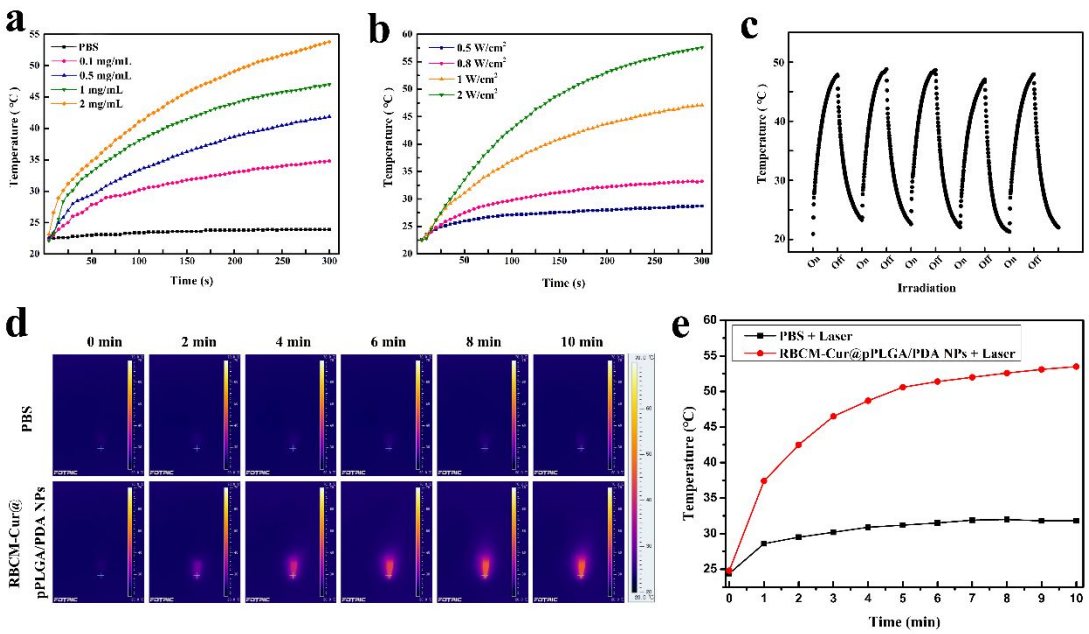

Figure 2. Temperature vs time plots of RBCM-Cur@pPLGA/PDA suspensions (a) at different concentrations under a laser power density of 1 W/cm^2 for 5 min, and (b) of a 1.0 mg/mL RBCM-Cur@pPLGA/PDA suspension exposed to varied laser power densities for 5 min. (c) A plot showing the temperature changes of an 1.0 mg/mL suspension of RBCM-Cur@pPLGA/PDA irradiated by an 808 nm laser (1.5 W/cm^2) over five on–off cycles. (d) Photothermal images and (e) temperature variation curves for PBS and the RBCM-Cur@pPLGA/PDA NPs (1.0 mg/mL) under continuous NIR laser irradiation (1 W/cm^2) for 10 min.

Drug release *in vitro*. The Cur EE%, LC% of the RBCM-Cur@PLGA/PDA NPs were found to be 75.5 ± 1.5% and 6.15 ± 0.6% w/w.

Drug release profiles are presented in Figure S6. The Cur@pPLGA/PDA NPs exhibited temperature- and H_2O_2-sensitive drug release. Curcumin was slowly released from the NPs in 37 ℃ PBS, with only ca. 23 ± 3% of the incorporated drug released after 48 h. However, more rapid and extensive drug release (*ca.* 66 ± 4% in 48 h) occurred at 45 ℃, which higher the Tg of PLGA NPs, and thus accelerated the degradation of the PLGA cores [36]. Moreover, a higher still release (more

than 87% in 48 h) was noted after adding 10 mM H_2O_2. This can be ascribed to the degradation of the PDA coating in the presence of H_2O_2. The conditions used here are representative of the intended therapeutic environment: 10 mM H_2O_2 is representative of the tumor microenvironment [32], and the temperature of the tumor will reach > 43 ºC during PTT. After RBCM coating, the drug release rate is mildly inhibited, which is ascribed to the external lipid bilayer blocking the curcumin release (resulting in *ca.* 80 ± 4% release after 48 h). These data confirm that the RBCM-Cur@pPLGA/PDA NPs can provide targeted drug release and should be able to eliminate off-targeted effects [8].

Cellular uptake *in vitro*. As depicted in Figure 3, strong curcumin (green) fluorescence was visible in the cells after they had been incubated for 2 h with the RBCM-Cur@pPLGA/PDA system. Minimal green fluorescence can be seen in the case of H22 cells treated with bare Cur@pPLGA/PDA NPs however. This is because of the presence of the RBCM cloaking on the NPs: both this and the cancer cell membrane comprise phospholipid bilayers, and thus there is enhanced endocytosis with the RBCM-coated formulation [37].

After incubation with the RBCM coated NPs, RAW264.7 cells showed only weak green fluorescence (Figure 3), however, greater uptake was observed using the uncoated Cur@pPLGA/PDA NPs. The lack of uptake by RAW264.7 (macrophage) cells arises because the expressed CD47 proteins of RBCM-coated nanoparticles from the RBCM at their exterior. This results in their selective uptake by cancer cells but not by phagocytic cells of immunity. The CD47 at the NP surface mimics the surface properties of the host cell, and the NPs thereby circumvent uptake by macrophages and send a "*don't eat me*" signal to the host [38]. Hence, the RBCM coating on the surface of the PLGA/PDA NPs is likely to extend their half life *in vivo* and thus to lead to more effective therapy of cancer.

The enhancement of H22 cell uptake with the RBCM coating is confirmed by flow cytometry (Figure S7). Uptake of RBCM-Cur@pPLGA/PDA NPs was found to be around 7.6-fold greater than with the uncoated analogue. This RBCM biomimetic camouflaging clearly contributes to highly specific cell uptake, avoiding the non-specific uptake which is typically seen with traditional surface modifications [39], and performs better than PEG or lipid coatings [22, 40].

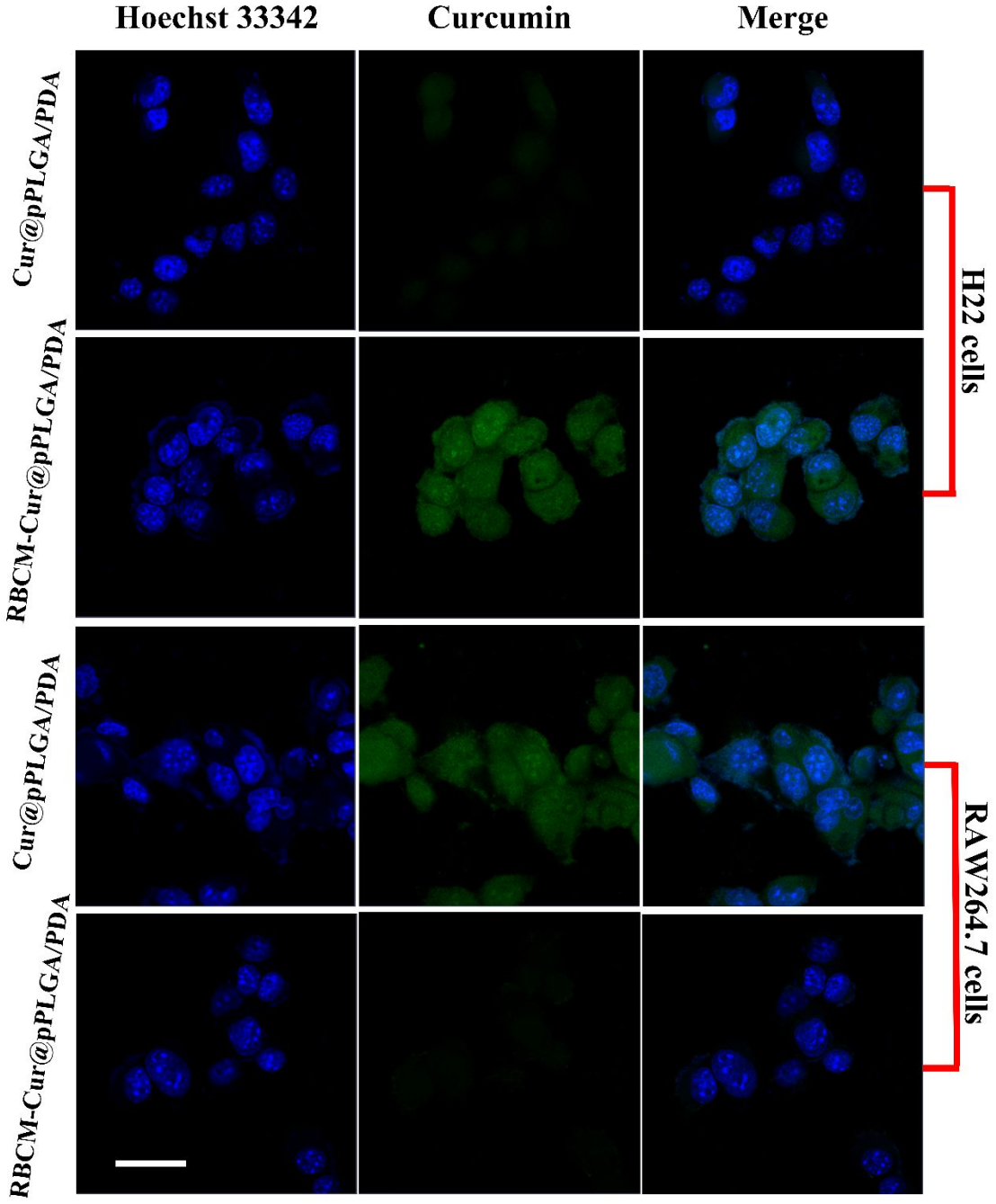

Figure 3. CLSM images of H22 cells and RAW264.7 cells following 2 h of exposure to

Cur@pPLGA/PDA or RBCM-Cur@pPLGA/PDA NPs. Scale bar: 20 μm.

***In vitro* cytotoxicity.** The cytocompatibility of the RBCM-pPLGA/PDA NPs was evaluated with L929 cells and H22 cells. As depicted in Fig. 4a and Figure 4b, the blank RBCM-pPLGA/PDA NPs had minimal effects on the viability of either healthy (L929) or cancerous (H22) cells. The cell viability was greater than 90%, even at concentrations of 500 μg/mL. The carrier material can thus be said to have good cytocompatibility.

Data for the cytotoxicity *in vitro* of the Cur-loaded formulations on H22 cells are given in Figure 4c. The half maximal inhibitory concentrations (IC50) of free curcumin, Cur@pPLGA/PDA NPs and RBCM-Cur@pPLGA/PDA NPs to H22 cells were calculated to be 14.66 μg/mL, 10.99 μg/mL and 8.13 μg/mL, respectively. Cell viability decreases with an increased concentration of curcumin, and at 20 μg/mL values of 40.7%, 35.5% and 25.8% were recorded for free Cur, Cur@pPLGA/PDA and RBCM-Cur@pPLGA/PDA NPs. Both sets of NPs are more effective at inducing cell death than free Cur, and the PDA shielded PLGA NPs could attribute to the endocytosis by cells [9], while the RBCM coating clearly enhances the cytotoxic effects of the nanoparticles. The addition of NIR irradiation further promoted cytotoxic activity, with the lowest cell viability of ~15% obtained using NIR and RBCM-Cur@pPLGA/PDA NPs at a Cur concentration of 20 μg/mL. Compared to a previous study in which we made similar particles loaded with curcumin but without PTT activity [41], the synergistic chemo-photothermal approach clearly affords improved antitumor efficacy.

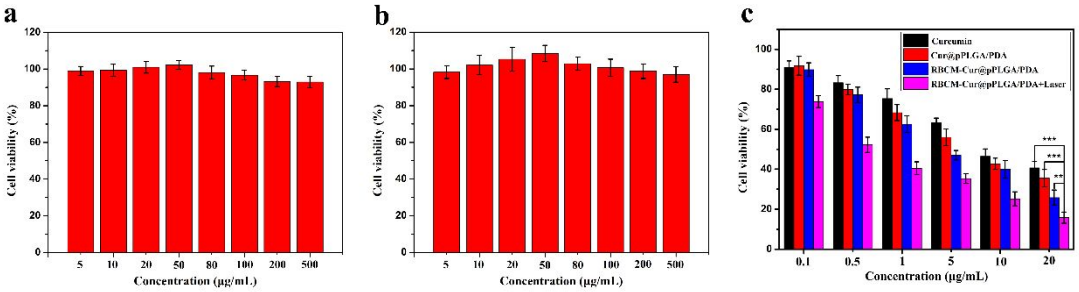

Figure 4. Cell viability data for (a) L929 cells and (b) H22 cells treated with different concentrations of RBCM-pPLGA/PDA NPs, in addition to (c) H22 cells treated with free curcumin, Cur@pPLGA/PDA NPs, RBCM-Cur@pPLGA/PDANPs, and RBCM-Cur@pPLGA/PDA + NIR irradiation at curcumin concentrations of 0.1–20 μg/mL. Data are presented as mean ± S.D. from three independent experiments (n=3).

Anti-tumor effects *in vivo.* The antitumor efficiency of the RBCM-Cur@pPLGA/PDA NPs was investigated in H22-tumor bearing ICR mice. The thermal images (Figure 5a and 5b) show that the RBCM-Cur@pPLGA/PDA NPs can quickly elevate the temperature of the tumor tissue to 43.8 °C within 5 min, and 46.5 ℃ within 10 min, while the tumor temperature of PBS-treated tumor-bearing mice increased by no more than 4.8 °C after NIR irradiation for 10 min. These results indicate that the RBCM-Cur@pPLGA/PDA NPs have potent *in vivo* photothermal effects and could potentially be used to ablate the tumor tissue.

Pharmacokinetic studies (Figure S8) demonstrate that the RBCM coated NPs had extended blood retention times compared to the bare NPs, with $t_{1/2}$ values of 6.6 and 10.7 h respectively. This finding confirms that the nanoparticles cloaked with the RBCM can provide long circulation times *in vivo*. These are favorable for enhanced tumor accumulation [42].

Treatement with RBCM-Cur@pPLGA/PDA NPs in combination with NIR irradiation inhibits tumor growth much more effectively than any other treatments explored (Figure 6a). Treatement with PBS, free Cur or the Cur@pPLGA/PDA NPs led to rapid growth of the tumor volume with

time, although the growth rate was reduced with the NPs. RBCM-Cur@pPLGA/PDA NP treatment led to a very modest rise in tumor volume, and with the addition of NIR irradiation the tumor volume did not change over the experimental period. This arises owing to the collaborative effect of chemo and photothermal therapy in the latter group. This is attributing to the RBCM coating both enhances the accumulation of the formulation in the tumor and uptake by cancer cells , as a result of the coating extending the systemic circulation time [38].

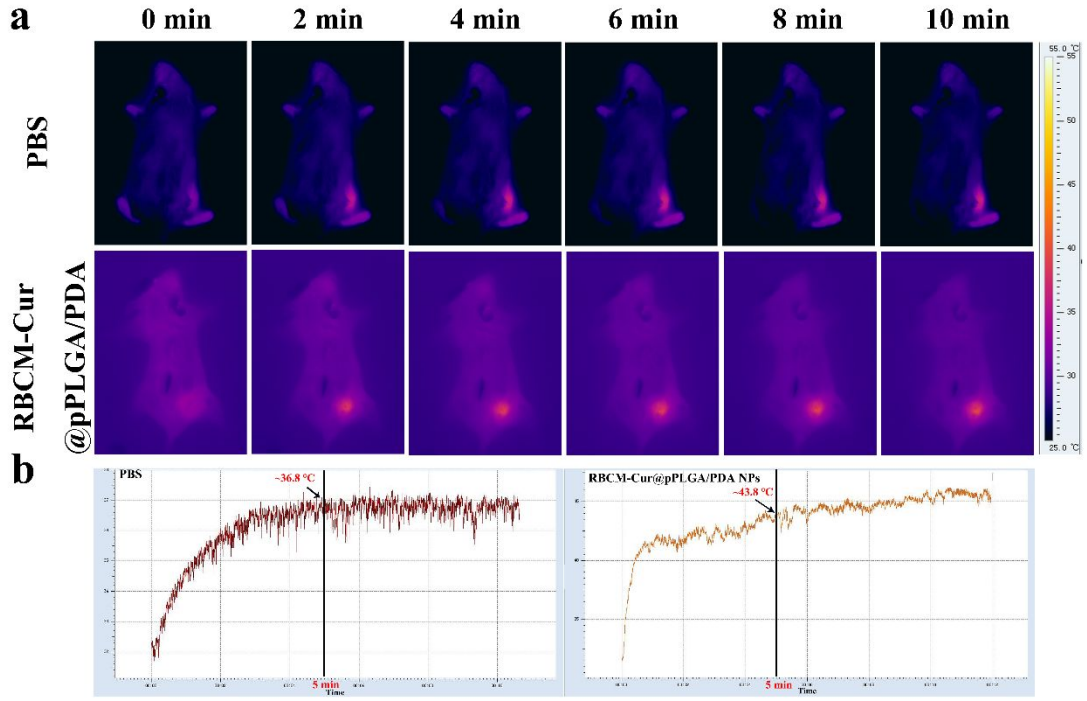

Figure 5. (a) Thermal images of mice after exposure to NIR irradiation for 10 min (2 W/cm^2) and (b) corresponding temperature variation curves.

The mice were sacrificed at the end of the experiment, the tumors were excised and weighed (Figure 6b and 6c): the masses lie in the order PBS > curcumin > Cur@pPLGA/PDA NPs > RBCM-Cur@pPLGA/PDA NPs > RBCM-Cur@pPLGA/PDA NPs + NIR. The body weight changes were also recorded (Figure 6d). In the case of the PBS group, the body weight of the mice increases over the experimental period, presumably because of tumor growth. Free curcumin treatment led to decreased body weights (by 4.3 ± 1.4%). The off-site toxicity and side effects arise with the free

drug was indicated. The mice treated with the uncoated NPs showed a small increase in body weight, while no notable changes in body weight were seen with the RBCM coated analogues.

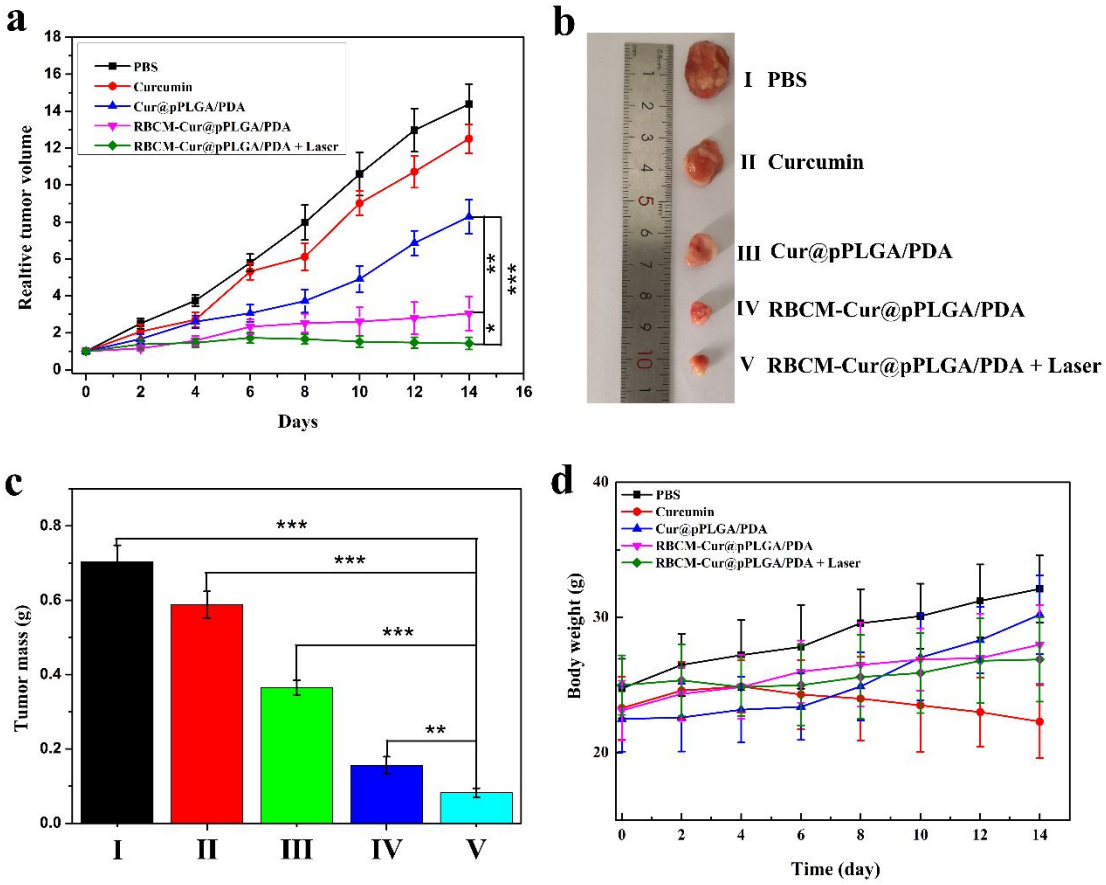

Figure 6. *In vivo* antitumor efficacy of the various formulations in the H22 tumor model. (a) H22 tumor growth curves after intravenous injection of different formulations. (b) Typical photographs of H22 tumor-bearing mice on day 14. (c) Mean weights of the H22 tumors isolated on day 14. (d) Body weight changes over the 14 days of the experiment. Quantitative data are given as mean ± S.D., n=5.

Histological analyses were performed to probe the apoptosis levels of the tumor tissues. H&E staining of tumor sections (Figure 7) demonstrated that RBCM-Cur@PLGA/PDA NPs caused the most severe tissue damage, particularly after NIR exposure, with the presence of swollen cell nuclei and crushed cells being more evident compared with slices from other groups. Animals treated with

free Cur show little change compared to the PBS control, while the NP formulations applied without laser treatment are intermediate between the two extremes. Apoptosis levels were further analyzed with the TUNEL assay. In the animals receiving curcumin or Cur@PLGA/PDA NPs, some green (apoptotic) cells can be seen, but apoptosis is much starker in the RBCM-Cur@PLGA/PDA NPs treatment group and is further promoted with additional laser treatment. These results clearly show that the RBCM-Cur@PLGA/PDA NPs can act as an efficient synergistic therapeutic agents for tumor suppression.

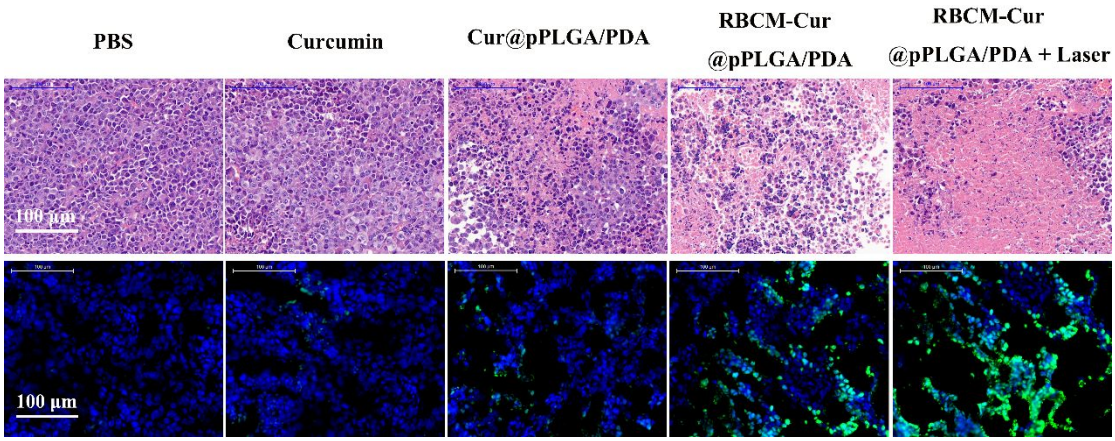

Figure 7. H&E staining (top) and TUNEL (bottom) images for tumors extracted after 14 days' treatment of the H22-tumor model animals. Representative images from each group are shown.

Safety evaluation. To evaluate the biocompatibility and *in vivo* safety of the RBCM-Cur@pPLGA/PDA NPs, the heart, liver, spleen, lung, and kidneys were recovered after sacrifice and imaged by H&E staining (Figure S9). The images are very similar for both the negative control group receiving PBS injections and the animals receiving RBCM-Cur@pPLGA/PDA NPs + Laser treatment. Hepatic (ALT and AST) and renal function (CREA and BUN) markers were also quantified. There are no significant differences between the RBCM-Cur@pPLGA/PDA NPs + Laser animals and the PBS control group (Fig. S10). The RBCM coated NPs are hence non-toxic

and safe for use *in vivo*.

Discussion. Chemo-photothermal therapy is one of the most widely explored combination therapies for cancer, and there have been many studies seeking to develop improved formulations for this. For example, Thapa. *et al*. developed zwitterion-coated gold-graphene oxide stealth nanovesicles for chemo-phototherapy in pancreatic cancer [43]. Potent antitumor effects were achieved in this work, but the non-biodegradable properties of the inorganic materials used is expected to limit clinical applications. The use of materials already approved by regulatory authorities is a much more promising approach if laboratory findings are to be translated into the clinic. Here, we prepare nanoparticles from the FDA-approved polymer PLGA and PDA. Both can biodegrade into nontoxic components, which ensures the *in vivo* biosafety of the NPs.

Many authors have explored the use of coating technologies to develop nano-scale drug delivery systems with high biocompatibility, low immunogenicity and prolonged blood circulation times. PEG or peptide surface modifiers comprise the current gold standard for endowing NPs with a "stealth" coating [44]. However, recent studies have shown that an anti-PEG immune response can be initiated [45], and often the targeting efficiency obtained with simple peptides is sub-optimal [37, 39]. To overcome these challenges, RBCM biomimetic nanoscale agents developed through top-down methods have attracted extensive research interest, resulting in materials with high biocompatibility, low immunogenicity, and long systemic circulation times [17, 37]. In this work, RBCM biomimetic PDA-coated NPs have been developed to deliver the chemotherapeutic drug curcumin and ensure effective passive targeted chemo-photothermal therapy. This strategy integrates biocompatible materials and a biomimetic RBCM surface, thereby overcoming many of the limitations of previously reported formulations.

CONCLUSIONS

In this study, curcumin loaded nanoparticles (NPs) were prepared with a porous PLGA core. This was coated with polydopamine, thereby endowing the particles with both chemotherapeutic and phothermal activity. The NPs were further coated with a "stealth" layer comprising the red blood cell membrane (RBCM), giving RBCM-Cur@pPLGA/PDA NPs. These had sizes around 200 nm, rendering them suitable for accumulation in a tumor by dint of the enhanced permeation and retention effect. The NPs further have excellent photothermal conversion capability (35.2%). While the blank carrier is highly cytocompatible, the drug-loaded system effectively induces cell death *in vitro*, particulary when the NPs are applied concomitantly with an NIR laser treatment. The RBCM coating enhances uptake by cancerous cells but discourages phagocytosis by macrophages, thus endowing the NPs with extended circulation times *in vivo* and the ability to target cancer cells. The RBCM-Cur@pPLGA/PDA NPs exhibit excellent antitumor efficacy in H22 tumor-bearing mice, and when applied with NIR irradiation lead to significant reductions in tumor volume without any off-target toxicity. Overall, our results demonstrate that the RBCM-Cur@pPLGA/PDA NPs comprise a biocompatible and effective therapeutic platform for *in vivo* chemo-photothermal combination treatment of cancer.

ASSOCIATED CONTENT

Supporting Information

The Supporting Information is available free of charge on the ACS Publications website.

N_2 adsorption/desorption isotherms and the pore-size distribution curves, FT-IR spectra, XPS spectra, SDS-PAGE analysis and Western blotting results, DLS sizes, curcumin release profiles, flow cytometry data together with fluorescence intensity quantification, pharmacokinetic data, and

H&E staining.

AUTHOR INFORMATION

Corresponding Authors

*E-mail: mailto:lzhu@dhu.edu.cn. Tel: +862167792655 (L.-M.Z.).

*E-mail: mailto:beached@126.com (J.Z.W.).

ORCID

Gareth R. Williams: 0000-0002-3066-2860

Li-Min Zhu: 0000-0003-2806-7971

Notes

The authors declare no competing financial interest.

ACKNOWLEDGEMENTS

This investigation was supported by grant 16410723700 from the Science and Technology Commission of Shanghai Municipality, the Biomedical Textile Materials “111 Project” of the Ministry of Education of China (No. B07024).

REFERENCES

1. Yang, K.; Feng, L.; Shi, X.; Liu, Z., Nano-graphene in biomedicine: theranostic applications. *Chem Soc Rev* **2013,** 42, (2), 530-47.

2. Lin, L. S.; Yang, X.; Niu, G.; Song, J.; Yang, H. H.; Chen, X., Dual-enhanced photothermal conversion properties of reduced graphene oxide-coated gold superparticles for light-triggered acoustic and thermal theranostics. *Nanoscale* **2016,** 8, (4), 2116-22.

3. Han, X.; Xu, Y.; Li, Y.; Zhao, X.; Zhang, Y.; Min, H.; Qi, Y.; Anderson, G. J.; You, L.; Zhao, Y.; Nie, G., An Extendable Star-Like Nanoplatform for Functional and Anatomical Imaging-Guided Photothermal Oncotherapy. *ACS Nano* **2019,** 13, (4), 4379-4391.

4. Thakur, N. S.; Patel, G.; Kushwah, V.; Jain, S.; Banerjee, U. C., Self-Assembled Gold Nanoparticle–Lipid Nanocomposites for On-Demand Delivery, Tumor Accumulation, and Combined Photothermal–Photodynamic Therapy. *ACS Applied Bio Materials* **2018,** 2, (1), 349-361.

5. Gao, W.; Li, S.; Liu, Z.; Sun, Y.; Cao, W.; Tong, L.; Cui, G.; Tang, B., Targeting and destroying tumor vasculature with a near-infrared laser-activated "nanobomb" for efficient tumor ablation. *Biomaterials* **2017,** 139, 1-11.

6. Zhu, X.; Ji, X.; Kong, N.; Chen, Y.; Mahmoudi, M.; Xu, X.; Ding, L.; Tao, W.; Cai, T.; Li, Y.; Gan, T.; Barrett, A.; Bharwani, Z.; Chen, H.; Farokhzad, O. C., Intracellular Mechanistic Understanding of 2D MoS2 Nanosheets for Anti-Exocytosis-Enhanced Synergistic Cancer Therapy. *ACS Nano* **2018,** 12, (3), 2922-2938.

7. He, H. C.; Markoutsa, E.; Zhan, Y. H.; Zhang, J. J.; Xu, P. S., Mussel-inspired PLGA/polydopamine core-shell nanoparticle for light induced cancer thermochemotherapy. *Acta Biomater.* **2017,** 59, 181-191.

8. Zhong, X.; Yang, K.; Dong, Z.; Yi, X.; Wang, Y.; Ge, C.; Zhao, Y.; Liu, Z., Polydopamine as a Biocompatible Multifunctional Nanocarrier for Combined Radioisotope Therapy and Chemotherapy of Cancer. *Adv. Funct. Mater.* **2015,** 25, (47), 7327-7336.

9. Ao, L.; Wu, C.; Liu, K.; Wang, W.; Fang, L.; Huang, L.; Su, W., Polydopamine-Derivated Hierarchical Nanoplatforms for Efficient Dual-Modal Imaging-Guided Combination in Vivo Cancer Therapy. *ACS Appl. Mater. Interfaces* **2018,** 10, (15), 12544-12552.

10. Chen, R.; Zhu, C.; Fan, Y.; Feng, W.; Wang, J.; Shang, E.; Zhou, Q.; Chen, Z., Polydopamine-Based Multifunctional Platform for Combined Photothermal Therapy, Chemotherapy, and Immunotherapy in Malignant Tumor Treatment. *ACS Applied Bio Materials* **2019,** 2, (2), 874-883.

11. Park, J.; Brust, T. F.; Lee, H. J.; Lee, S. C.; Watts, V. J.; Yeo, Y., Polydopamine-based simple and versatile surface modification of polymeric nano drug carriers. *ACS nano* **2014,** 8, (4), 3347-3356.

12. Zeng, J.; Shi, D.; Gu, Y.; Kaneko, T.; Zhang, L.; Zhang, H.; Kaneko, D.; Chen, M., Injectable and Near-Infrared-Responsive Hydrogels Encapsulating Dopamine-Stabilized Gold Nanorods with Long Photothermal Activity Controlled for Tumor Therapy. *Biomacromolecules* **2019,** 20, (9), 3375-3384.

13. Ryu, J. H.; Messersmith, P. B.; Lee, H., Polydopamine Surface Chemistry: A Decade of Discovery. *ACS Appl Mater Interfaces* **2018,** 10, (9), 7523-7540.

14. Lee, H.; Dellatore, S. M.; Miller, W. M.; Messersmith, P. B., Mussel-inspired surface chemistry for multifunctional coatings. *Science* **2007,** 318, (5849), 426-430.

15. Vader, P.; van der Aa, L. J.; Engbersen, J. F.; Storm, G.; Schiffelers, R. M., Physicochemical and biological evaluation of siRNA polyplexes based on PEGylated Poly(amido amine)s. *Pharm*

Res **2012,** 29, (2), 352-61.

16. Zhu, J.; Zhang, M.; Zheng, D.; Hong, S.; Feng, J.; Zhang, X.-Z., A universal approach to render nanomedicine with biological identity derived from cell membranes. *Biomacromolecules* **2018,** 19, (6), 2043-2052.

17. Zhou, J.; Kroll, A. V.; Holay, M.; Fang, R. H.; Zhang, L., Biomimetic Nanotechnology toward Personalized Vaccines. *Adv. Mater.* **2019**, e1901255.

18. Han, X.; Wang, C.; Liu, Z., Red Blood Cells as Smart Delivery Systems. *Bioconjug Chem* **2018**. 29, (4), 852-860.

19. Hu, Q.; Bomba, H. N.; Gu, Z., Engineering platelet-mimicking drug delivery vehicles. *Front. Chem. Sci. Eng.* **2017,** 11, (4), 624-632.

20. Wang, H.; Wu, J.; Williams, G. R.; Fan, Q.; Niu, S.; Wu, J.; Xie, X.; Zhu, L. M., Platelet-membrane-biomimetic nanoparticles for targeted antitumor drug delivery. *J Nanobiotechnology* **2019,** 17, (1), 60.

21. Wang, H.; Bremner, D. H.; Wu, K.; Gong, X.; Fan, Q.; Xie, X.; Zhang, H.; Wu, J.; Zhu, L.-M., Platelet membrane biomimetic bufalin-loaded hollow MnO_2 nanoparticles for MRI-guided chemo-chemodynamic combined therapy of cancer. *Chem. Eng. J.* **2020,** 382, 122848.

22. Gao, M.; Liang, C.; Song, X.; Chen, Q.; Jin, Q.; Wang, C.; Liu, Z., Erythrocyte-Membrane-Enveloped Perfluorocarbon as Nanoscale Artificial Red Blood Cells to Relieve Tumor Hypoxia and Enhance Cancer Radiotherapy. *Adv. Mater.* **2017,** 29, (35), 1701429.

23. Fu, Y.; Liu, W.; Wang, L. Y.; Zhu, B. Y.; Qu, M. K.; Yang, L. Q.; Sun, X.; Gong, T.; Zhang, Z. R.; Lin, Q.; Zhang, L., Erythrocyte-Membrane-Camouflaged Nanoplatform for Intravenous Glucose-Responsive Insulin Delivery. *Adv. Funct. Mater.* **2018,** 28, (41), 1802250.

24. Gao, M.; Liang, C.; Song, X. J.; Chen, Q.; Jin, Q. T.; Wang, C.; Liu, Z., Erythrocyte-Membrane-Enveloped Perfluorocarbon as Nanoscale Artificial Red Blood Cells to Relieve Tumor Hypoxia and Enhance Cancer Radiotherapy. *Adv. Mater.* **2017,** 29, (35), 1701429.

25. Hu, C. M. J.; Zhang, L.; Aryal, S.; Cheung, C.; Fang, R. H.; Zhang, L. F., Erythrocyte membrane-camouflaged polymeric nanoparticles as a biomimetic delivery platform. *P. Natl. Acad. Sci. USA.* **2011,** 108, (27), 10980-10985.

26. Schurch, C. M.; Forster, S.; Bruhl, F.; Yang, S. H.; Felley-Bosco, E.; Hewer, E., The "don't eat me" signal CD47 is a novel diagnostic biomarker and potential therapeutic target for diffuse malignant mesothelioma. *Oncoimmunology* **2017,** 7, (1), e1373235.

27. Kim, H. Y.; Cho, E. J.; Chun, S.; Kim, K. H.; Cho, D., Red Blood Cell Alloimmunization in Korean Patients With Myelodysplastic Syndrome and Liver Cirrhosis. *Ann. Lab. Med.* **2019,** 39, (2), 218-222.

28. Rapido, F.; Brittenham, G. M.; Bandyopadhyay, S.; La Carpia, F.; L'Acqua, C.; McMahon, D. J.; Rebbaa, A.; Wojczyk, B. S.; Netterwald, J.; Wang, H. L.; Schwartz, J.; Eisenberger, A.; Soffing, M.; Yeh, R.; Divgi, C.; Ginzburg, Y. Z.; Shaz, B. H.; Sheth, S.; Francis, R. O.; Spitalnik, S. L.; Hod, E. A., Prolonged red cell storage before transfusion increases extravascular hemolysis. *J. Clin. Invest.* **2017,** 127, (1), 375-382.

29. Salvagno, G. L.; Sanchis-Gomar, F.; Picanza, A.; Lippi, G., Red blood cell distribution width: A simple parameter with multiple clinical applications. *Crit. Rev. Cl. Lab. Sci.* **2015,** 52, (2), 86-105.

30. Zhu, H. J.; Chen, H. B.; Zeng, X. W.; Wang, Z. Y.; Zhang, X. D.; Wu, Y. P.; Gao, Y. F.; Zhang, J. X.; Liu, K. W.; Liu, R. Y.; Cai, L. T.; Mei, L.; Feng, S. S., Co-delivery of chemotherapeutic drugs

with vitamin E TPGS by porous PLGA nanoparticles for enhanced chemotherapy against multi-drug resistance. *Biomaterials* **2014,** 35, (7), 2391-2400.

31. Hu, C. M. J.; Fang, R. H.; Wang, K. C.; Luk, B. T.; Thamphiwatana, S.; Dehaini, D.; Nguyen, P.; Angsantikul, P.; Wen, C. H.; Kroll, A. V.; Carpenter, C.; Ramesh, M.; Qu, V.; Patel, S. H.; Zhu, J.; Shi, W.; Hofman, F. M.; Chen, T. C.; Gao, W. W.; Zhang, K.; Chien, S.; Zhang, L. F., Nanoparticle biointerfacing by platelet membrane cloaking. *Nature* **2015,** 526, (7571), 118-121.

32. Bao, X.; Zhao, J.; Sun, J.; Hu, M.; Yang, X., Polydopamine Nanoparticles as Efficient Scavengers for Reactive Oxygen Species in Periodontal Disease. *ACS Nano* **2018,** 12, (9), 8882-8892.

33. Wang, D.; Wu, H.; Lim, W. Q.; Phua, S. Z. F.; Xu, P.; Chen, Q.; Guo, Z.; Zhao, Y., A Mesoporous Nanoenzyme Derived from Metal-Organic Frameworks with Endogenous Oxygen Generation to Alleviate Tumor Hypoxia for Significantly Enhanced Photodynamic Therapy. *Adv. Mater.* **2019**, e1901893.

34. Wang, J.; Zhu, C.; Han, J.; Han, N.; Xi, J.; Fan, L.; Guo, R., Controllable synthesis of gold nanorod/conducting polymer core/shell hybrids toward in vitro and in vivo near-infrared photothermal therapy. *ACS appl. Mater. Interfaces* **2018,** 10, (15), 12323-12330.

35. Lyu, Y.; Xie, C.; Chechetka, S. A.; Miyako, E.; Pu, K., Semiconducting polymer nanobioconjugates for targeted photothermal activation of neurons. *J. Am. Chem. Soc.* **2016,** 138, (29), 9049-9052.

36. Zolnik, B. S.; Burgess, D. J., Effect of acidic pH on PLGA microsphere degradation and release. *J Control Release* **2007,** 122, (3), 338-44.

37. Hu, C. M.; Zhang, L.; Aryal, S.; Cheung, C.; Fang, R. H.; Zhang, L., Erythrocyte membrane-

camouflaged polymeric nanoparticles as a biomimetic delivery platform. *Proc Natl Acad Sci U S A* **2011,** 108, (27), 10980-5.

38. Chambers, E.; Mitragotri, S., Long circulating nanoparticles via adhesion on red blood cells: Mechanism and extended circulation. *Experimental Biology and Medicine* **2007,** 232, (7), 958-966.

39. Cui, L.; Lin, Q.; Jin, C. S.; Jiang, W.; Huang, H.; Ding, L.; Muhanna, N.; Irish, J. C.; Wang, F.; Chen, J.; Zheng, G., A PEGylation-Free Biomimetic Porphyrin Nanoplatform for Personalized Cancer Theranostics. *ACS Nano* **2015,** 9, (4), 4484-95.

40. Shi, J.; Kantoff, P. W.; Wooster, R.; Farokhzad, O. C., Cancer nanomedicine: progress, challenges and opportunities. *Nat Rev Cancer* **2017,** 17, (1), 20-37.

41. Xie, X.; Wang, H.; Williams, G. R.; Yang, Y.; Zheng, Y.; Wu, J.; Zhu, L. M., Erythrocyte Membrane Cloaked Curcumin-Loaded Nanoparticles for Enhanced Chemotherapy. *Pharmaceutics* **2019,** 11, (9), 429.

42. Zeng, X.; Liu, G.; Tao, W.; Ma, Y.; Zhang, X.; He, F.; Pan, J.; Mei, L.; Pan, G., A drug-self-gated mesoporous antitumor nanoplatform based on pH-sensitive dynamic covalent bond. *Adv. Funct. Mater.* **2017,** 27, (11), 1605985.

43. Thapa, R. K.; Ku, S. K.; Choi, H. G.; Yong, C. S.; Byeon, J. H.; Kim, J. O., Vibrating droplet generation to assemble zwitterion-coated gold-graphene oxide stealth nanovesicles for effective pancreatic cancer chemo-phototherapy. *Nanoscale* **2018,** 10, (4), 1742-1749.

44. Davis, M. E.; Chen, Z.; Shin, D. M., Nanoparticle therapeutics: an emerging treatment modality for cancer. In *Nanoscience And Technology: A Collection of Reviews from Nature Journals*, World Scientific: 2010; pp 239-250.

45. Knop, K.; Hoogenboom, R.; Fischer, D.; Schubert, U. S., Poly(ethylene glycol) in drug

delivery: pros and cons as well as potential alternatives. *Angew Chem Int Ed Engl* **2010,** 49, (36), 6288-308.

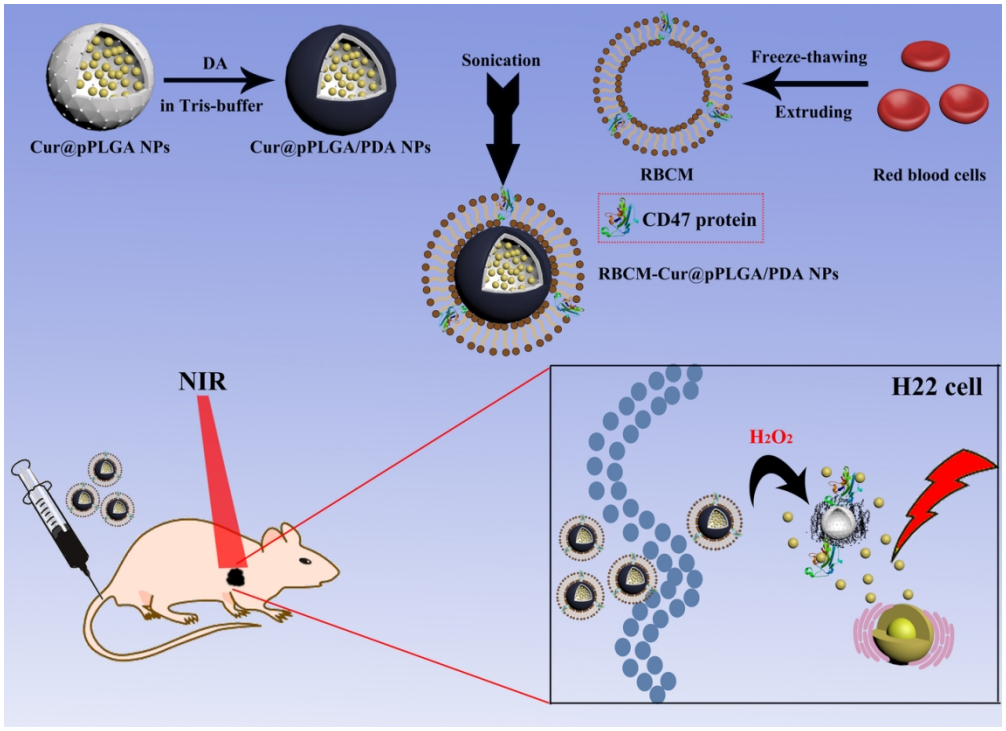

119x86mm (300 x 300 DPI)